Sensors and Actuators: A. Physical 332 (2021) 113136

Contents lists available at ScienceDirect

Sensors and Actuators: A. Physical

journal homepage: www.elsevier.com/locate/sna

Key role of high-T_c twinned martensitic materials to gain a magnetic actuation higher than 15%

Numan Şarlı[a,*], Nejdet Paran[a,b], Günyaz Ablay[b], Hamza Y. Ocak[c], Yasin G. Yıldız[d], Gökçen D. Yıldız[e], Nermin K. Yağcı[e]

[a] Department of Physics, Erciyes University, 38039 Kayseri, Turkey
[b] Department of Electrical and Electronics Engineering, Abdullah Gül University, 38080 Kayseri, Turkey
[c] Department of Physics, Dumlupınar University, 43100 Kütahya, Turkey
[d] Department of Electronics and Automation, Kırıkkale University, 71100 Kırıkkale, Turkey
[e] Department of Physics, Kırıkkale University, 71450 Kırıkkale, Turkey

ARTICLE INFO

Article history:
Received 28 April 2021
Received in revised form 18 August 2021
Accepted 22 September 2021
Available online 28 September 2021

Keywords:
Actuator
Sensor
Strain
Magnetic field
Twinning angle
Effective field theory

ABSTRACT

Twinning angle outcomes of the twinned martensitic (TM) and detwinned martensitic (DTM) structural transformations on the magnetic features of the austenite (A) parent phase are researched by using the effective field theory established by Kaneyoshi. The implementation of the effective field theory verifies that the shape memory mechanism occurs with phase transformations, A→TM→DTM→A. It also shows that the austenite parent phase has two types of actuations: one-dimensional actuation (in only y-axis) for TM, and two-dimensional actuation (in x and y-axes) for DTM. Magnetic field-induced actuation (strain) in the range of 5–15% at twinning angle $\theta \geq 120.816°$ of TM and DTM is reported for some materials in the literature. On the other hand, in this work, it is estimated that a twinning angle lower than this twinning angle (i.e., $\theta < 120.816°$) must be achieved to have a strain higher than 15%. We also suggest that materials with higher magnetization, Curie temperature, coercive field and remanence magnetization should be taken into account to get a strain higher than 15%, since all these features are directly affected by the twinning angle (θ). Our results on Curie temperature (T_c) match with the experimental results of $Ni_{49.8}Mn_{28.5}Ga_{21.7}$ (achieved 6% strain) with T_c = 95 °C (368 K) by Murray et al., and $Ni_{46}Mn_{24}Ga_{22}Co_4Cu_4$ with T_c = 393 K (achieved 12% strain) by Sozinov et al.

1. Introduction

Magnetic shape memory alloys (MSMAs) are able to generate forces and encounter deformations under a magnetic field. The other most important classes of MSMSAs are magnetostrictive materials and piezoelectric ceramics. Magnetostrictive materials are deformed under an applied magnetic field, while piezoelectric ceramics encounter mechanical strain under an applied electrical field [1–3]. Because MSMAs have unique properties of generating some percent of magnetic field induced strain (MFIS), it has many possibilities for applications in sensor design, harvesters, magnetic refrigeration systems, biomedical, actuators, and numerous other technological applications [4,5]. The temperatures of the martensitic phase transition are the reason that MSMAs can be used for purpose of engineering [6,7]. MSMAs are able to offer some novel innovative applications operating at frequencies that cannot be accomplished with traditional shape memory alloys [8]. The working mechanism relies on rearrangement of the crystallographic domains with the external magnetic field. Thus, a large strain is obtained similar to a stress-induced one [9,10]. Ni-Mn-Ga crystals have given the best results so far, so they are getting a great deal of attention in research community because of their high potentials [11,12]. Ni_2MnGa is a potential new class of MSMAs materials, which deforms to the ferromagnetic martensite phase under an applied magnetic field. The applied magnetic field can easily affect the martensite transformation in Ni_2MnGa [13]. The meta-magnetic shape memory alloys such as NiCoMnIn is capable of converting magnetic Zeeman energy into mechanical force, and thus they are the subject of a widespread research [14]. The MSM effects can be classified into two categories; the effects observed in a twinned magnetically ordered material, and the effects lead to a magnetoelastic phase transition steered by magnetic fields [15]. There is also a multistable actuator solution that can be used in different fluidic applications including mobile or

* Corresponding author.
E-mail address: numansarli82@gmail.com (N. Şarlı).

https://doi.org/10.1016/j.sna.2021.113136
0924-4247/

stationary hydraulics and pneumatics [16]. MSMAs encounter a martensitic phase transformation under cooling such that an austenite (high symmetry) phase transforms to a martensite (low symmetry) phase [17]. The MSMA is in the austenite crystallographic phase at high temperatures, but the martensite phase appears when it is cooled down [18]. Ni_2MnGa can also be used for transducers design which is a very important part of every mechatronic device [19]. MSMAs are one of the novel materials for various types of sensors and micro-actuators [20], because they are capable of providing precise and fast movements under suitable excitations [21].

A handful approach for modeling magnetic systems and analyzing their magnetic features is the effective field theory (EFT) proposed by Kaneyoshi [22]. EFT is also used to model some physical effects and phenomena recently. For example, quantum tunneling effect of magnetization [23], structural transformation based exchange bias effect [24], the magnetocaloric effect [25], lattice location effect [26], transverse field effect of Aluminum concentration [27], spin orientation effect [28,29], perpendicular magnetic anisotropy effect explained by c/a ratio [30], Bain thermal magnetization loop [31] and Bain spin memory effect [32], minimum Curie temperature effect [33], bridge constant and atom in magnetism in Ni_2MnSb Heusler alloy [34], intersection magnetism and intersection temperature [35], zero internal energy and minimum internal energy broken [36], type II superconductivity [37–42], surface superconductivity [43], applied transverse field effects on the antiferromagnetic properties of the Ising nanoparticles [44], structural effects on the magnetic and thermodynamic properties of the monolayer graphdiyne-like [45], center decorated hexagon and tetragon structures [46], and soft magnetic characteristics [47], were examined with EFT. While the EFT is a quite useful tool for modeling magnetic systems with certain lattice structures, there is only one work in the literature that models the austenite and martensite structural transformations with this method [48]. However, in Ref. [48], magnetic properties (M-T and M-H curves) are studied at only one constant twinning angle ($\theta = 120°$). The twinning angle effect ($0° < \theta < 180°$) and actuation (strain) have not been modeled and investigated so far. Therefore, this paper aims to model the twinning angle effect and actuation and to investigate their effects on the magnetic and structural properties of the martensitic phase transformations using the EFT theory.

2. Theoretical background

The A, TM and DTM phases are modeled with EFT and their corresponding formulations were given in our previous work [48]. In this work a similar procedure will be applied to model the twinning angle effect and actuation.

Fig. 1 illustrates the A, TM and DTM structures, which are obtained from the literature of structural transformation in shape memory effect [48–52]. The mathematical expressions for the A, TM, and DTM are written as follows [48]:

Hamiltonian for Austenite (A);

$$\begin{aligned} H_A = &- J_{a1} \sum_{\langle m1,m1\rangle} S^z_{m1}S^z_{m1} - J_{a2} \sum_{\langle m1,m3\rangle} S^z_{m1}S^z_{m3} - J_{a3} \sum_{\langle m1,m3\rangle} S^z_{m1}S^z_{m3} \\ &- J_{a4} \sum_{\langle m3,m3\rangle} S^z_{m3}S^z_{m3} - J_{a5} \sum_{\langle m3,m5\rangle} S^z_{m3}S^z_{m5} - J_{a6} \sum_{\langle m3,m5\rangle} S^z_{m3}S^z_{m5} \\ &- J_{a7} \sum_{\langle m5,m5\rangle} S^z_{m5}S^z_{m5} - h\left(\sum_{m1} S^z_{m1} + \sum_{m3} S^z_{m3} + \sum_{m5} S^z_{m5}\right) \end{aligned} \quad (1)$$

Magnetizations for A;

$$\begin{aligned} m1_A &= [\cosh(J_{a1}\nabla) + m1_A \sinh(J_{a1}\nabla)]^1 [\cosh(J_{a2}\nabla) + m3_A \sinh(J_{a2}\nabla)]^1 \\ &\quad [\cosh(J_{a3}\nabla) + m3_A \sinh(J_{a3}\nabla)]^1 F_{s-1/2}(x)|_{x=0}, m3_A \\ &= [\cosh(J_{a2}\nabla) + m1_A \sinh(J_{a2}\nabla)]^1 [\cosh(J_{a3}\nabla) + m1_A \sinh(J_{a3}\nabla)]^1 \\ &\quad [\cosh(J_{a4}\nabla) + m3_A \sinh(J_{a4}\nabla)]^1 [\cosh(J_{a5}\nabla) + m5_A \sinh(J_{a5}\nabla)]^1 \\ &\quad [\cosh(J_{a6}\nabla) + m5_A \sinh(J_{a6}\nabla)]^1 F_{s-1/2}(x)|_{x=0}, m5_A \\ &= [\cosh(J_{a5}\nabla) + m3_A \sinh(J_{a5}\nabla)]^2 [\cosh(J_{a6}\nabla) + m3_A \sinh(J_{a6}\nabla)]^2 \\ &\quad [\cosh(J_{a7}\nabla) + m5_A \sinh(J_{a7}\nabla)]^1 F_{s-1/2}(x)|_{x=0}, \end{aligned} \quad (2)$$

Hamiltonian for twinned martensite (TM);

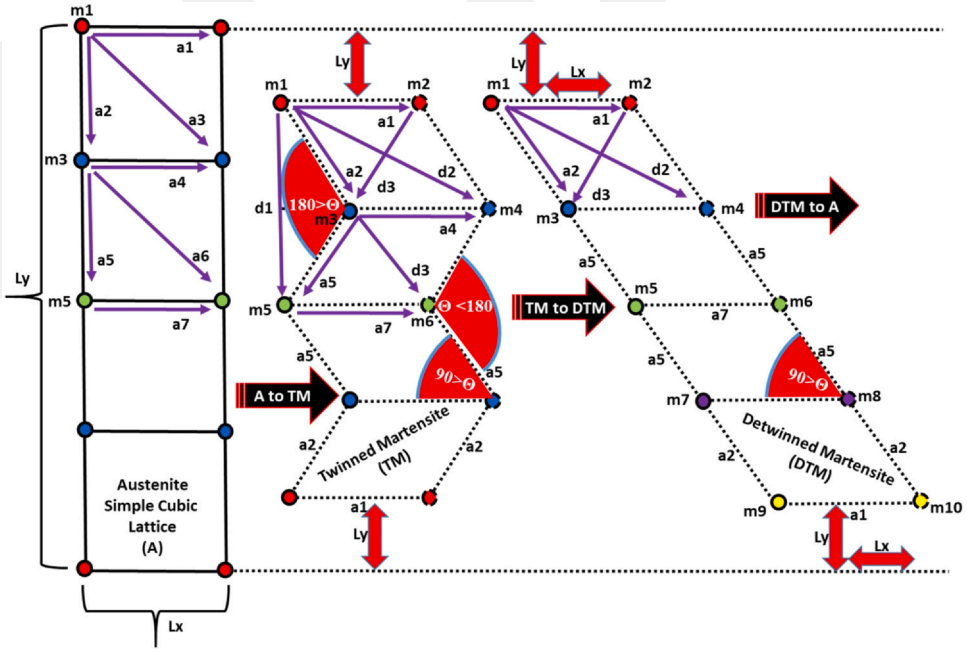

Fig. 1. The illustrative diagram of the actuation in the austenite (A), twinned martensite (TM) and detwinned (or deformed) martensite (DTM) structures [48–52].

$$H_{TM} = -J_{a1}\sum_{\langle m1,m2\rangle} S^z_{m1}S^z_{m2} - J_{a2}\sum_{\langle m1,m3\rangle} S^z_{m1}S^z_{m3} - J_{a4}\sum_{\langle m3,m4\rangle} S^z_{m3}S^z_{m4} - J_{a5}\sum_{\langle m3,m5\rangle} S^z_{m3}S^z_{m5} - J_{a7}\sum_{\langle m5,m6\rangle} S^z_{m5}S^z_{m5} - J_{d1}\sum_{\langle m1,m5\rangle} S^z_{m1}S^z_{m5} - J_{d2}\sum_{\langle m1,m4\rangle} S^z_{m1}S^z_{m4} - J_{d3}\sum_{\langle m2,m3\rangle} S^z_{m2}S^z_{m3} - h\left(\sum_{m1} S^z_{m1} + \sum_{m2} S^z_{m2} + \sum_{m3} S^z_{m3} + \sum_{m4} S^z_{m4} + \sum_{m5} S^z_{m5} + \sum_{m6} S^z_{m6}\right), \quad (3)$$

Magnetizations for TM;

$$\begin{aligned}
m1_{TM} &= [\cosh(J_{a1}\nabla) + m2_{TM}\sinh(J_{a1}\nabla)]^1[\cosh(J_{a2}\nabla) + m3_{TM}\sinh(J_{a2}\nabla)]^1 \\
&\quad [\cosh(J_{d2}\nabla) + m4_{TM}\sinh(J_{d2}\nabla)]^1 \\
&\quad [\cosh(J_{d1}\nabla) + m5_{TM}\sinh(J_{d1}\nabla)]^1 F_{s-1/2}(x)|_{x=0}, \\
m2_{TM} &= [\cosh(J_{a1}\nabla) + m1_{TM}\sinh(J_{a1}\nabla)]^1[\cosh(J_{d3}\nabla) + m3_{TM}\sinh(J_{d3}\nabla)]^1 \\
&\quad [\cosh(J_{a2}\nabla) + m4_{TM}\sinh(J_{a2}\nabla)]^1 \\
&\quad [\cosh(J_{d1}\nabla) + m6_{TM}\sinh(J_{d1}\nabla)]^1 F_{s-1/2}(x)|_{x=0}, \\
m3_{TM} &= [\cosh(J_{a2}\nabla) + m1_{TM}\sinh(J_{a2}\nabla)]^1[\cosh(J_{d3}\nabla) + m2_{TM}\sinh(J_{d3}\nabla)]^1 \\
&\quad [\cosh(J_{d1}\nabla) + m3_{TM}\sinh(J_{d1}\nabla)]^1 \\
&\quad [\cosh(J_{a4}\nabla) + m4_{TM}\sinh(J_{a4}\nabla)]^1[\cosh(J_{a5}\nabla) + m5_{TM}\sinh(J_{a5}\nabla)]^1 \\
&\quad [\cosh(J_{d3}\nabla) + m6_{TM}\sinh(J_{d3}\nabla)]^1 F_{s-1/2}(x)|_{x=0}, \\
m4_{TM} &= [\cosh(J_{d2}\nabla) + m1_{TM}\sinh(J_{d2}\nabla)]^1[\cosh(J_{a2}\nabla) + m2_{TM}\sinh(J_{a2}\nabla)]^1 \\
&\quad [\cosh(J_{a4}\nabla) + m3_{TM}\sinh(J_{a4}\nabla)]^1 \\
&\quad [\cosh(J_{d1}\nabla) + m4_{TM}\sinh(J_{d1}\nabla)]^1[\cosh(J_{d2}\nabla) + m5_{TM}\sinh(J_{d2}\nabla)]^1 \\
&\quad [\cosh(J_{a5}\nabla) + m6_{TM}\sinh(J_{a5}\nabla)]^1 F_{s-1/2}(x)|_{x=0}, \\
m5_{TM} &= [\cosh(J_{d1}\nabla) + m1_{TM}\sinh(J_{d1}\nabla)]^2[\cosh(J_{a2}\nabla) + m2_{TM}\sinh(J_{a2}\nabla)]^1 \\
&\quad [\cosh(J_{a5}\nabla) + m3_{TM}\sinh(J_{a5}\nabla)]^1 \\
&\quad [\cosh(J_{d2}\nabla) + m4_{TM}\sinh(J_{d2}\nabla)]^2[\cosh(J_{a7}\nabla) + m6_{TM}\sinh(J_{a7}\nabla)]^1 \\
&\quad F_{s-1/2}(x)|_{x=0}, \\
m6_{TM} &= [\cosh(J_{d1}\nabla) + m2_{TM}\sinh(J_{d1}\nabla)]^2[\cosh(J_{d3}\nabla) + m3_{TM}\sinh(J_{d3}\nabla)]^2 \\
&\quad [\cosh(J_{a5}\nabla) + m4_{TM}\sinh(J_{a5}\nabla)]^1 \\
&\quad [\cosh(J_{a2}\nabla) + m4_{TM}\sinh(J_{a2}\nabla)]^1[\cosh(J_{a7}\nabla) + m5_{TM}\sinh(J_{a7}\nabla)]^1 \\
&\quad F_{s-1/2}(x)|_{x=0},
\end{aligned} \quad (4)$$

Hamiltonian for detwinned martensite (DTM);

$$H_{DTM} = -J_{a1}\sum_{\langle m1,m2\rangle} S^z_{m1}S^z_{m2} - J_{a2}\sum_{\langle m1,m3\rangle} S^z_{m1}S^z_{m3} - J_{a4}\sum_{\langle m3,m4\rangle} S^z_{m3}S^z_{m4} - J_{a5}\sum_{\langle m3,m5\rangle} S^z_{m3}S^z_{m5} - J_{a7}\sum_{\langle m5,m6\rangle} S^z_{m5}S^z_{m6} - J_{d2}\sum_{\langle m1,m4\rangle} S^z_{m1}S^z_{m4} - J_{d2}\sum_{\langle m3,m6\rangle} S^z_{m3}S^z_{m6} - J_{d2}\sum_{\langle m5,m8\rangle} S^z_{m5}S^z_{m8} - J_{d2}\sum_{\langle m7,m10\rangle} S^z_{m7}S^z_{m10} - J_{d3}\sum_{\langle m2,m3\rangle} S^z_{m2}S^z_{m3} - J_{d3}\sum_{\langle m4,m5\rangle} S^z_{m4}S^z_{m5} - J_{d3}\sum_{\langle m6,m7\rangle} S^z_{m6}S^z_{m7} - J_{d3}\sum_{\langle m8,m9\rangle} S^z_{m8}S^z_{m9} - h\left(\sum_{m1} S^z_{m1} + \sum_{m2} S^z_{m2} + \sum_{m3} S^z_{m3} + \sum_{m4} S^z_{m4} + \sum_{m5} S^z_{m5} + \sum_{m6} S^z_{m6} + \sum_{m7} S^z_{m7} + \sum_{m8} S^z_{m8} + \sum_{m9} S^z_{m9} + \sum_{m10} S^z_{m10}\right), \quad (5)$$

Magnetizations for DTM;

$$\begin{aligned}
m1_{DTM} &= [\cosh(J_{a1}\nabla) + m2_{DTM}\sinh(J_{a1}\nabla)]^1[\cosh(J_{a2}\nabla) + m3_{DTM}\sinh(J_{a2}\nabla)]^1 \\
&\quad [\cosh(J_{d2}\nabla) + m4_{DTM}\sinh(J_{d2}\nabla)]^1 F_{s-1/2}(x)|_{x=0}, \\
m2_{DTM} &= [\cosh(J_{a1}\nabla) + m1_{DTM}\sinh(J_{a1}\nabla)]^1[\cosh(J_{a2}\nabla) + m4_{DTM}\sinh(J_{a2}\nabla)]^1 \\
&\quad [\cosh(J_{d3}\nabla) + m3_{DTM}\sinh(J_{d3}\nabla)]^1 F_{s-1/2}(x)|_{x=0}, \\
m3_{DTM} &= [\cosh(J_{a2}\nabla) + m1_{DTM}\sinh(J_{a2}\nabla)]^1[\cosh(J_{a4}\nabla) + m4_{DTM}\sinh(J_{a4}\nabla)]^1 \\
&\quad [\cosh(J_{a5}\nabla) + m5_{DTM}\sinh(J_{a5}\nabla)]^1[\cosh(J_{d3}\nabla) + m2_{DTM}\sinh(J_{d3}\nabla)]^1 \\
&\quad [\cosh(J_{d2}\nabla) + m6_{DTM}\sinh(J_{d2}\nabla)]^1 F_{s-1/2}(x)|_{x=0}, \\
m4_{DTM} &= [\cosh(J_{a2}\nabla) + m2_{DTM}\sinh(J_{a2}\nabla)]^1[\cosh(J_{a4}\nabla) + m3_{DTM}\sinh(J_{a4}\nabla)]^1 \\
&\quad [\cosh(J_{a5}\nabla) + m6_{DTM}\sinh(J_{a5}\nabla)]^1[\cosh(J_{d2}\nabla) + m1_{DTM}\sinh(J_{d2}\nabla)]^1 \\
&\quad [\cosh(J_{d3}\nabla) + m5_{DTM}\sinh(J_{d3}\nabla)]^1 F_{s-1/2}(x)|_{x=0}, \\
m5_{DTM} &= [\cosh(J_{a5}\nabla) + m3_{DTM}\sinh(J_{a5}\nabla)]^1[\cosh(J_{a5}\nabla) + m7_{DTM}\sinh(J_{a5}\nabla)]^1 \\
&\quad [\cosh(J_{a7}\nabla) + m6_{DTM}\sinh(J_{a7}\nabla)]^1[\cosh(J_{d3}\nabla) + m4_{DTM}\sinh(J_{d3}\nabla)]^1 \\
&\quad [\cosh(J_{d2}\nabla) + m8_{DTM}\sinh(J_{d2}\nabla)]^1 F_{s-1/2}(x)|_{x=0}, \\
m6_{DTM} &= [\cosh(J_{a5}\nabla) + m4_{DTM}\sinh(J_{a5}\nabla)]^1[\cosh(J_{a5}\nabla) + m8_{DTM}\sinh(J_{a5}\nabla)]^1 \\
&\quad [\cosh(J_{a7}\nabla) + m5_{DTM}\sinh(J_{a7}\nabla)]^1[\cosh(J_{d3}\nabla) + m7_{DTM}\sinh(J_{d3}\nabla)]^1 \\
&\quad [\cosh(J_{d2}\nabla) + m3_{DTM}\sinh(J_{d2}\nabla)]^1 F_{s-1/2}(x)|_{x=0}, \\
m7_{DTM} &= [\cosh(J_{a5}\nabla) + m5_{DTM}\sinh(J_{a5}\nabla)]^1[\cosh(J_{a2}\nabla) + m9_{DTM}\sinh(J_{a2}\nabla)]^1 \\
&\quad [\cosh(J_{a4}\nabla) + m8_{DTM}\sinh(J_{a4}\nabla)]^1[\cosh(J_{d3}\nabla) + m6_{DTM}\sinh(J_{d3}\nabla)]^1 \\
&\quad [\cosh(J_{d2}\nabla) + m10_{DTM}\sinh(J_{d2}\nabla)]^1 F_{s-1/2}(x)|_{x=0}, \\
m8_{DTM} &= [\cosh(J_{a5}\nabla) + m6_{DTM}\sinh(J_{a5}\nabla)]^1[\cosh(J_{a2}\nabla) + m10_{DTM}\sinh(J_{a2}\nabla)]^1 \\
&\quad [\cosh(J_{a4}\nabla) + m7_{DTM}\sinh(J_{a4}\nabla)]^1[\cosh(J_{d3}\nabla) + m9_{DTM}\sinh(J_{d3}\nabla)]^1 \\
&\quad [\cosh(J_{d2}\nabla) + m5_{DTM}\sinh(J_{d2}\nabla)]^1 F_{s-1/2}(x)|_{x=0}, \\
m9_{DTM} &= [\cosh(J_{a1}\nabla) + m10_{DTM}\sinh(J_{a1}\nabla)]^1[\cosh(J_{a2}\nabla) + m7_{DTM}\sinh(J_{a2}\nabla)]^1 \\
&\quad [\cosh(J_{d3}\nabla) + m8_{DTM}\sinh(J_{d3}\nabla)]^1 F_{s-1/2}(x)|_{x=0}, \\
m10_{DTM} &= [\cosh(J_{a1}\nabla) + m9_{DTM}\sinh(J_{a1}\nabla)]^1[\cosh(J_{a2}\nabla) + m8_{DTM}\sinh(J_{a2}\nabla)]^1 \\
&\quad [\cosh(J_{d2}\nabla) + m7_{DTM}\sinh(J_{d2}\nabla)]^1 F_{s-1/2}(x)|_{x=0},
\end{aligned} \quad (6)$$

In the Hamiltonians, $S^z = \pm 1$ denotes Pauli spin operator, and the external magnetic field is denoted by h. The coefficients a_i (i = 1–7) and d_i (i = 1–3) denote the distance between the two nearest-and next-nearest-neighbor atoms. J_{ai} (i = 1–7) and J_{di} (i = 1–3) represent the exchange interaction between two nearest-and next-nearest-neighbor atoms, and the values of the J are calculated from the relationship $J_i = k_i/n_{di}$ [38–48,53]. The parameters a and d are related to the lattice constants (a = 1 Å, d depends on the shearing angle). The normalized lattice constants are given by $n_{ai} = a/1$ Å and $n_{di} = di/1$ Å. k denotes a constant, and J is ferromagnetic if k = 1 > 0, and J is antiferromagnetic if k = −1 < 0. Reduced Js values are given in Table 1 for k = 1.

The terms used in the magnetizations include the differential operator $\nabla = \partial/\partial x$ and $F_{1/2}(x)$ is given for the spin-1/2 particles described as [48],

$$F_{1/2}(x) = \tanh[\beta(x + h)], \quad (7)$$

where k_B is the Boltzmann's constant, $\beta = 1/k_BT_A$, and absolute temperature is given by T_A. In the calculations the reduced temperature, $T = k_BT_A/J$, and the reduced applied field, i.e. H = h/J, are used. Finally, the equations for total magnetization of the A, TM, and DTM are written as follow [48],

$$\begin{aligned}
MT_A &= \frac{1}{10}(4m1_A + 4m3_A + 2m5_A). \\
MT_{TM} &= \frac{1}{10}(2m1_{TM} + 2m2_{TM} + 2m3_{TM} + 2m4_{TM} + m5_{TM} + m6_{TM}), \\
MT_{DTM} &= \frac{1}{10}(m1_{DTM} + m2_{DTM} + m3_{DTM} + m4_{DTM} + m5_{DTM} \\
&\quad + m6_{DTM} + m7_{DTM} + m8_{DTM} + m9_{DTM} + m10_{DTM}).
\end{aligned} \quad (8)$$

3. Numerical results and discussion

Fig. 1 shows the twinned martensite (TM) and detwinned martensite (DTM) structure obtained from the austenite (A) phase with

Table 1
Reduced exchange interactions of the A, TM and DTM.

Js vs θ°	25°	50°	75°	100°	125°	150°	175°
J_{a1}	1	1	1	1	1	1	1
J_{a2}	1	1	1	1	1	1	1
J_{a3}	0.707101	0.707101	0.707101	0.707101	0.707101	0.707101	0.707101
J_{a4}	1	1	1	1	1	1	1
J_{a5}	1	1	1	1	1	1	1
J_{a6}	0.707101	0.707101	0.707101	0.707101	0.707101	0.707101	0.707101
J_{a7}	1	1	1	1	1	1	1
J_{d1}	2.31011	1.1831	0.82134	0.652704	0.563691	0.517638	0.500476
J_{d2}	0.50299	0.51214	0.528022	0.551689	0.584856	0.630236	0.692172
J_{d3}	4.59277	2.31011	1.5555	1.1831	0.963812	0.82134	0.723052

the twinning angle. The austenite parent phase has two types of actuations. One of them is the one-dimensional actuation obtained from the TM (only in L_y-axis), and the other one is the two-dimensional actuation obtained from the DTM (both in L_y- and L_x-axis) as seen in Fig. 1. These two types of actuations occur because of the nature of the transformation from A to TM and transformation from A to DTM structures (i.e., from the nature of shape memory mechanism). This structural transformation mechanism is seen in Fig. 1 as A→TM→DTM→A.

Fig. 2 shows the twinning angle dependence of the thermal magnetization (M-T curves) of the austenite (A), twinned martensite (TM), and detwinned martensite (DTM) structures at H = 0.00. In Fig. 2(a)–(g), M-T curves of the A (solid line), TM (dotted line) and DTM (dashed line) are obtained for the twinning angles of θ = 25–175° with a 25° step, respectively. The thermal magnetization loop areas between A, TM and DTM decrease as the twinning angle increases. The loop area between A and DTM is smaller than that of the A and TM. Since the shape memory mechanism occurs as A→TM→DTM→A, these results are quite meaningful. It is clearly seen that the loop area between A and DTM is almost zero when the twinning angle is θ = 175° (see Fig. 2(g)). This result demonstrates that the DTM phase transforms to the A-phase when the twinning angle is θ = 180°. Therefore, M-T curves of the A and DTM overlap at this twinning angle.

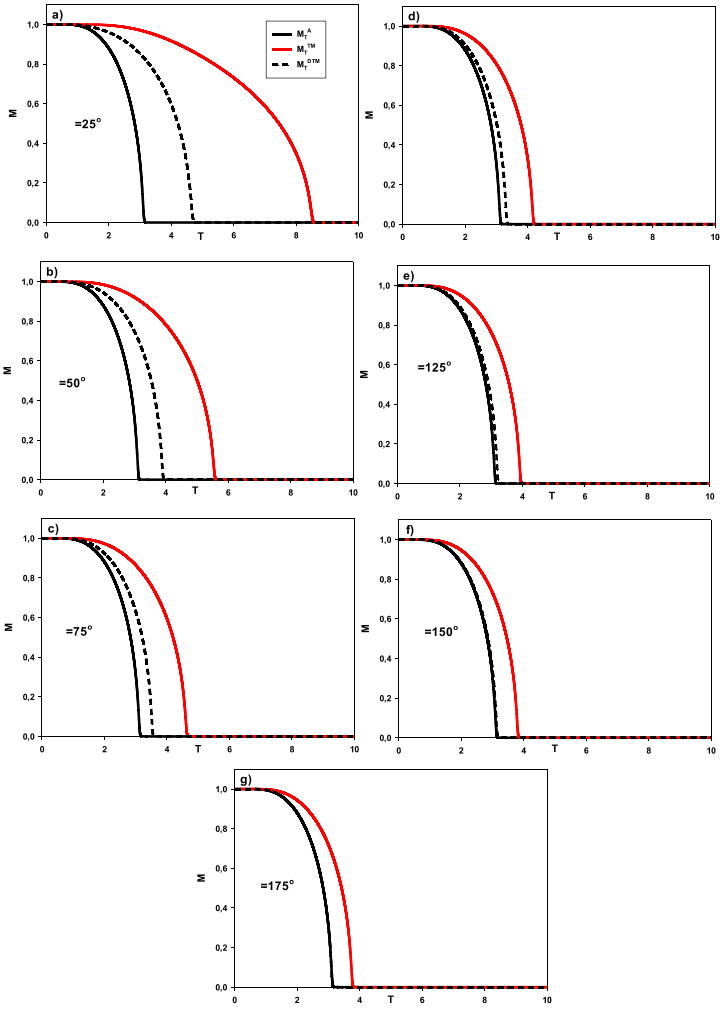

Fig. 2. Relationship of the thermal magnetization of austenite (A), twinned martensite (TM) and detwinned martensite (DTM) structures with twinning angles.

Fig. 3 shows the twinning angle dependence of the Curie temperature (T_c-θ curves) and length shifting (actuation in L_x- and L_y-axis) of the austenite (A), twinned martensite (TM) and detwinned martensite (DTM) structures. In Fig. 3(a), T_c of the A (solid line) is obtained as T_c = 3.2 (A phase is independent of the θ). T_c of the TM (dotted line) is obtained as T_c = 8.64, 5.66, 4.71, 4.26, 4.02, 3.89 and 3.84 for the twinning angle of θ = 25°, 50°, 75°, 100°, 125°, 150° and 175°, respectively. T_c of the DTM (dashed line) is obtained as T_c = 4.8, 3.99, 3.61, 3.4, 3.28, 3.22 and 3.19 for the twinning angle of θ = 25°, 50°, 75°, 100°, 125°, 150° and 175°, respectively. It is observed that the T_c of the TM and DTM decreases as θ increases. Similarly, the T_c value of DTM is approaching to that of A and they overlap for the higher twinning angles (θ = 175°). On the other hand, the T_c values of the A and TM are separate from each other and they do not overlap for the higher twinning angle (θ = 175°). In Fig. 3(b), length shifting (actuation in L_y-axis) of the A and TM is obtained. One-dimensional length shifting (actuation in only L_y-axis (dotted line)) is obtained for the TM. The original normalized length of the L_y-axis of the A is 4. The length shifting of the TM (red line) in L_y is obtained as L_y = 0.8657, 1.6904, 2.1492, 3.0641, 3.5480, 3.8637 and 3.9961 for the twinning angle of θ = 25°, 50°, 75°, 100°, 125°, 150° and 175°, respectively. On the other hand, L_x = 0 for TM. It is obviously seen that the length of the L_y-axis of the TM is almost the same with the A phase for the higher twinning angle (θ = 175°). Thus, they recover and remember their original shape of A phase. This is the base of the magnetic actuation with the shape memory effect. At this point, by using our theoretical model we can predict the range of the twinning angle of the magnetic actuation of materials reported in the literature.

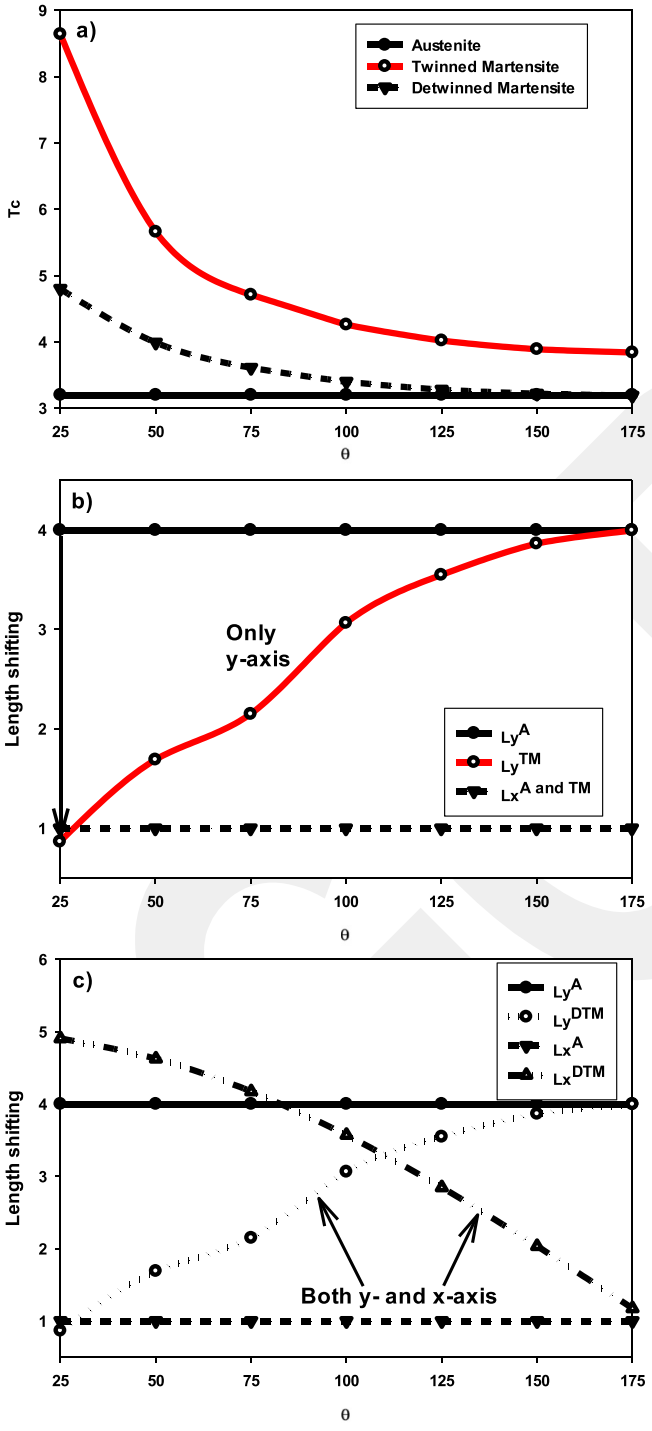

Fig. 3. Twinning angle (θ) vs Curie temperature (T_c) of the A, TM and DTM structures (a); length shifting of A and TM (b); length shifting of A and DTM (c). (For interpretation of the references to color in this figure legend, the reader is referred to the web version of this article.)

Up to now, the magnetic field-induced strain (actuation) nearly between 5% and 15% has been reported for some materials at the range of 125–150° twinning angles [3,4]. In our system, this strain between 5% and 15% is obtained when L_y takes values between 3.80952 (4/1.05) and 3.47826 (4/1.15) with a twinning angle θ ≥ 120.816°. In addition, as also indicated in our previous work [48], for the given twinning angle θ = 120° (≈ 120.816°), the Curie temperature values are obtained as T_c^A = 3.2, T_c^{TM} = 4.05 and T_c^{DTM} = 3.3, and the coercive field points are obtained as H_c^A = 1.01, H_c^{TM} = 1.61 and H_c^{DTM} = 1.07 at T = 1. These numerical results suggest that a strain higher than 15% (4/1.15001 > 4/1.15000) can be obtained for a twinning angle lower than 120.816°, higher curie temperatures than T_c^A = 3.2, T_c^{TM} = 4.05 and T_c^{DTM} = 3.3, and higher coercive field points than H_c^A = 1.01, H_c^{TM} = 1.61 and H_c^{DTM} = 1.07.

Our numerical results of T_c are in good agreement with the experimental results provided by Murray et al. [3] and Sozinov et al. [4] Murray et al. [3] achieved 6% strain for $Ni_{49.8}Mn_{28.5}Ga_{21.7}$ single crystals with a Curie temperature of T_c = 95 °C (368 K). On the other hand, Sozinov et al. [4] achieved 12% strain for $Ni_{46}Mn_{24}Ga_{22}Co_4Cu_4$ single variant sample with a Curie temperature of T_c = 393 K. By considering these experimental studies, it is obvious that strain increases from 6% to 12% when T_c increases from 368 K to 398 K. These reported experimental results confirm our numerical findings on T_c which provides a higher actuation (or strain). However, since magnetization (M), Curie temperature (T_c), coercive field (H_c) and remanence magnetization (M_r) obtained by EFT strongly depend on twinning angle (θ), one should take into account the twinned materials with higher M, T_c, H_c and M_r to gain a strain higher than 15%.

4. Conclusions

Twinning angle effects of the twinned martensitic (TM) and detwinned martensitic (DTM) structural transformations on the magnetic features of the austenite (A) parent phase are investigated using EFT. We find that;

1. One-dimensional magnetic actuation is obtained from the twinned martensite whereas two-dimensional actuation is obtained from the detwinned martensite.
2. The thermal magnetization loop areas between A, TM and DTM decrease as the twinning angle increases.
3. The loop area between the A and DTM is smaller than that of the A and TM.
4. The T_c of the A and DTM are almost same and they overlap for the higher twinning angle (θ = 175°).

5. The T_c of the A and TM are separate from each other and they do not overlap for the higher twinning angle ($\theta = 175°$).
6. The length of the L_y-axis of the TM and DTM is almost the same with the A phase for the higher twinning angle ($\theta = 175°$). Thus, they recover and remember their original shape of A phase.
7. The thermal magnetization (M), Curie temperature (T_c) and length shifting (L_x, L_y) discrepancies between A and DTM become zero about $\theta \approx 180°$. This confirms that the shape memory mechanism occurs with the phase transformation A→TM→DTM→A.
8. Magnetization (M), Curie temperature (T_c), coercive field (H_c) and remanence magnetization (M_r) obtained by EFT strongly depend on twinning angle (θ). Hence, the twinned materials with higher M, T_c, H_c and M_r values should be considered to gain a strain higher than 15%.
9. Our suggestion on T_c is in good agreement with the experimental T_c results of $Ni_{49.8}Mn_{28.5}Ga_{21.7}$ by Murray et al. [3] and $Ni_{46}Mn_{24}Ga_{22}Co_4Cu_4$ by Sozinov et al. [4] to gain a strain from 6% (Tc = 368 K) to 12% (Tc = 393 K).

CRediT authorship contribution statement

Numan Şarlı: Software. **Günyaz Ablay:** Formal analysis, Writing – review & editing, Writing – original draft. **Nejdet Paran:** Resources. **Hamza Y. Ocak:** Conceptualization, Supervision, Validation. **Yasin G. Yıldız:** Methodology. **Gökçen D. Yıldız:** Visualization, Data curation. **Nermin K. Yağcı:** Investigation.

Declaration of Competing Interest

The authors declare that they have no known competing financial interests or personal relationships that could have appeared to influence the work reported in this paper.

Acknowledgments

The authors declare that there is no conflict of interest.

References

[1] J. Tellinen, I. Suorsa, I. Aaltio, K. Ullakko, Basic Properties of Magnetic Shape Memory Actuators, 2002, pp. 10–12.
[2] K. Ullakko, Magnetically controlled shape memory alloys: a new class of actuator materials, J. Mater. Eng. Perform. 5 (1996) 405–409.
[3] S.J. Murray, M. Marioni, S.M. Allen, R.C. O'Handley, T.A. Lograsso, 6% Magnetic-field-induced strain by twin-boundary motion in ferromagnetic Ni-Mn-Ga, Appl. Phys. Lett. 77 (2000) 886–888.
[4] A. Sozinov, N. Lanska, A. Soroka, W. Zou, 12% Magnetic field-induced strain in Ni-Mn-Ga-based non-modulated martensite, Appl. Phys. Lett. 102 (2013) 021902.
[5] B. Kiefer, D.C. Lagoudas, Magnetic field-induced martensitic variant reorientation in magnetic shape memory alloys, Philos. Mag. 85 (2005) 4289–4329.
[6] P. Zhao, J. Cullen, M. Wuttig, Actuation field in martensitic Ni49.0 Mn23.5 Ga27.5, J. Appl. Phys. 101 (2007) 09C519.
[7] C.M. Craciunescu, I. Mitelea, V. Budau, Actuation micro-design based on martensitic phase transformations in shape memory alloys, in: AIP Conf. Proc., American Institute of Physics AIP, 2012, pp. 135–140.
[8] S. Faehler, An introduction to actuation mechanisms of magnetic shape memory alloys, ECS Trans. 3 (2019) 155–163.
[9] A. Sozinov, A.A. Likhachev, N. Lanska, K. Ullakko, Giant magnetic-field-induced strain in NiMnGa seven-layered martensitic phase, Appl. Phys. Lett. 80 (2002) 1746–1748.
[10] E. Pagounis, R. Chulist, M.J. Szczerba, M. Laufenberg, High-temperature magnetic shape memory actuation in a Ni-Mn-Ga single crystal, Scr. Mater. 83 (2014) 29–32.
[11] P. Müllner, V.A. Chernenko, G. Kostorz, Large cyclic magnetic-field-induced deformation in orthorhombic (14M) Ni-Mn-Ga martensite, J. Appl. Phys. 95 (2004) 1531–1536.
[12] E. Pagounis, M.J. Szczerba, R. Chulist, M. Laufenberg, Large magnetic field-induced work output in a NiMnGa seven-layered modulated martensite, Appl. Phys. Lett. 107 (2015) 152407.
[13] X. Jin, D. Bono, R.C. O'Handley, S.M. Allen, T.Y. Hsu, Magnetic field effects on strain and resistivity during the martensitic transformation in Ni-Mn-Ga single crystals, J. Appl. Phys. 93 (2003) 8630–8632.
[14] N.M. Bruno, S. Wang, I. Karaman, Y.I. Chumlyakov, Reversible martensitic transformation under low magnetic fields in magnetic shape memory alloys, Sci. Rep. 7 (2017) 40434.
[15] S. Rößler, C. Koz, Z. Wang, Y. Skourski, M. Doerr, D. Kasinathan, H. Rosner, M. Schmidt, U. Schwarz, U.K. Rößler, S. Wirth, Two types of magnetic shape-memory effects from twinned microstructure and magneto-structural coupling in $Fe_{1+y}Te$, Proc. Natl. Acad. Sci. USA 116 (2019) 16697–16702.
[16] T. Schiepp, E. Pagounis, M. Laufenberg, Magnetic shape memory actuators for fluidic applications, in: Proceedings of the 9th International Fluid Power Conference, 9. IFK, March 24–26, Aachen, Germany, 2014.
[17] H.C. Xuan, L.J. Shen, T. Tang, Q.Q. Cao, D.H. Wang, Y.W. Du, Magnetic-field-induced reverse martensitic transformation and large magnetoresistance in Ni50−xCoxMn32Al18 Heusler alloys, Appl. Phys. Lett. 100 (2012) 172410.
[18] J.Y. Gauthier, A. Hubert, J. Abadie, N. Chaillet, C. Lexcellent, J.Y. Gauthier, A. Hubert, J. Abadie, N. Chaillet, Magnetic shape memory alloy and actuator design, in: Proceedings of the 5th International Workshop on Microfactories, IWMF'06, Besançon, France, 2006.
[19] B. Minorowicz, A. Nowak, F. Stefański, Position regulation of magnetic shape memory actuator, J. Ach. Mater. Manuf. Eng. 61 (2013) 216–221.
[20] S.A. Wilson, R.P.J. Jourdain, Q. Zhang, R.A. Dorey, C.R. Bowen, M. Willander, Q.U. Wahab, M. Willander, S.M. Al-hilli, O. Nur, E. Quandt, C. Johansson, E. Pagounis, M. Kohl, J. Matovic, B. Samel, W. van der Wijngaart, E.W.H. Jager, D. Carlsson, Z. Djinovic, M. Wegener, C. Moldovan, E. Abad, M. Wendlandt, C. Rusu, K. Persson, New materials for micro-scale sensors and actuators. An engineering review, Mater. Sci. Eng. R Rep. 56 (2007) 1–129.
[21] L. Riccardi, G. Ciaccia, D. Naso, H. Janocha, B. Turchiano, Position control for a magnetic shape memory actuator, in: Proceedings of the IFAC Proc. Vol., IFAC Secretariat, 2010, pp. 478–485.
[22] T. Kaneyoshi, Differential operator technique in the Ising spin systems, Acta Phys. Pol. A 83 (1993) 703–737.
[23] G.D. Yıldız, Y.G. Yıldız, N. Şarlı, Spin induced quantum tunneling of the magnetization, SPIN 11 (2021) 2150011.
[24] Y.G. Yıldız, Exchange bias effect revealed by irreversible structural transformation between the HCP and FCC structures of Cobalt nanoparticles, Phase Trans. 93 (2020) 429–437.
[25] Ü. Akıncı, Magnetocaloric properties of the binary Ising model with arbitrary spin, J. Magn. Magn. Mater. 523 (2021) 167625.
[26] A. Duran, Lattice location effect of $Ni_{50}Mn_{36}Sn_{14}$ Heusler alloy, J. Supercond. Nov. Magn. 31 (2017) 1101–1109.
[27] H.Y. Ocak, G.D. Yıldız, Y.G. Yıldız, B. Saatçi, R. Basar, G. Sarıoglu, Transverse field effects of Al concentration on magnetic properties of B2-FeAl nanoparticle, Acta Phys. Pol. A 139 (2021) 20–24.
[28] N. Şarlı, Generation of an external magnetic field with the spin orientation effect in a single layer Ising nanographene, Physica E 83 (2016) 22–29.
[29] N. Şarlı, Artificial magnetism in a carbon diamond nanolattice with the spin orientation effect, Diam. Relat. Mater. 64 (2016) 103–109.
[30] N.K. Yağcı, Perpendicular magnetic anisotropy revealed by c/a ratio of Mn_2NiB Heusler alloy, J. Supercond. Nov. Magn. 34 (2021) 959–962.
[31] N. Şarlı, Y. Dağdemir, B. Saatçi, Small thermal magnetization loop revealed by Bain Strain, J. Supercond. Nov. Magn. 32 (2019) 3933–3938.
[32] B. Saatçi, N. Şarlı, Y. Dağdemir, Y.G. Yıldız, H.Y. Ocak, Prediction of the Bain spin memory materials (BSMM) revealed by Kaneyoshi theory, Phase Trans. 100 (2020) 330–339.
[33] Y.G. Yıldız, Origin of the hardness in the monolayer nanographene, Phys. Lett. A 383 (2019) 2333–2338.
[34] B. Saatçi, N. Şarlı, E.G. Özdemir, Z. Merdan, Bridge constant and atom between theoretical and experimental magnetism in Ni_2MnSb Heusler alloy: DFT and EFT studies, Philos. Mag. B 101 (2021) 501–516.
[35] G.D. Yıldız, Intersection magnetization and temperature revealed by FCC-FCT phase transformation in the FePd binary alloy system, J. Supercond. Nov. Magn. 33 (2020) 2051–2058.
[36] N.K. Yağcı, Magnetic properties of the David star in the 2D-Kagome lattice, Philos. Mag. B 101 (2020) 1019–1032.
[37] I.T. Padilha, J. Ricardo de Sousa, M.A. Neto, O.R. Salmon, J.R. Viana, Thermodynamics properties of copper-oxide superconductors described by an Ising frustrated model, Physica A 392 (2013) 4897–4904.
[38] M. Keskin, N. Şarlı, Superconducting phase diagram of the yttrium, barium and YBa-core in YBCO by an Ising model, JEPT 127 (2018) 516–524.
[39] N. Şarlı, M. Keskin, Effects of the copper and oxygen atoms of the CuO-plane on magnetic properties of the YBCO by using the effective-field theory, Chin. J. Phys. 59 (2019) 256–264.
[40] N. Şarlı, M. Keskin, Effect of the distance range between the YBa-core and CuO-shell on the superconducting properties in the YBCO by an Ising model, Chin. J. Phys. 63 (2020) 375–381.
[41] E. Kantar, Superconductivity-like phenomena in anferrimagnetic endohedral fullerene with diluted magnetic surface, Solid State Commun. 263 (2017) 31–37.
[42] A. Duran, Magnetic properties of Mn_2RhSi Heusler alloy: phase transition and hysteresis behavior at a very low temperature, J. Low. Temp. Phys. 203 (2021) 127–142.
[43] A. Duran, Surface superconductivity in $Ni_{50}Mn_{36}Sn_{14}$ Heusler alloy, J. Supercond. Nov. Magn. 31 (2018) 4053–4062.
[44] T. Kaneyoshi, Magnetism in an antiferromagnetic Ising nanoparticle under an applied transverse field, Chem. Phys. Lett. 736 (2019) 136755.
[45] N. Si, Y.L. Zhang, W. Jiang, Magnetic and thermodynamic properties of monolayer graphdiyne-like, Comput. Mater. Sci. 197 (2021) 110594.

[46] J.Q. Hu, N. Si, W. Jiang, J. Meng, Y.L. Zhang, Magnetic and thermodynamic properties of center decorated hexagon and tetragon structures, Phys. Lett. A 405 (2021) 127434.
[47] A. Duran, Soft magnetic characteristic of Ni50Mn36Sn14 Heusler alloy, cukurovaummfd 33 (2018) 139–152.
[48] N. Şarlı, G.D. Yıldız, Y.G. Yıldız, N.K. Yağcı, Magnetic properties of the martensitic transformations with twinned and detwinned, Physica B 553 (2019) 161–168.
[49] S. Jiang, J. Yu, L. Hu, Y. Zhang, Investigation on deformation mechanisms of NiTi shape memory alloy tube under radial loading, Metals 7 (2017) 268–278.
[50] M. Woo Han, H. Rodrigue, S. Cho, S. Hyuk Song, W. Wang, W.S. Chu, S.H. Ahn, Woven type smart soft composite for soft morphing car spoiler, Compos. Part B 86 (2016) 285–298.
[51] S. Barbarino, E.I. Saavedra Flores, R.M. Ajaj, I. Dayyani, M.I. Friswell, A review on shape memory alloys with applications to morphing aircraft, Smart Mater. Struct. 23 (2014) 063001.
[52] M. Fabrizioa, M. Pecorarob, V. Tibullob, A shape memory alloy model by a second order phase transition, Mech. Res. Commun. 74 (2016) 20–26.
[53] C. Kittel, Introduction to Solid State Physics, seventh ed., John Wiley & Sons, Inc, New York, 1996, pp. 333–378.

Numan Şarlı received his M.S. and B.S. degrees in physics from the Kafkas University, and Ph.D. degree from the Erciyes University. He is currently working as researcher at the Erciyes University. His research focuses on software, model and design, Ising spin systems, magnetism, effective field theory.

Nejdet Paran received his B.S. and M.S. degrees in Physics from the Erciyes University. He is currently pursuing a Ph.D. degree in physics at the Abdullah Gül University. His research focuses on robotics, designing an electronics board, Photomultiplier Tubes.

Günyaz Ablay received his Ph.D. degree in Nuclear Engineering from the Ohio State University, and his M.S. and B.S. degrees in Electrical-Electronics Engineering from Firat University. He is currently working as Associate Professor at the Abdullah Gul University. His research interests include control theory and its applications, embedded control, robotics, chaos theory and nuclear energy technologies.

Hamza Yaşar Ocak received his B.S. degrees in Physics from the Atatürk University, M.S. and Ph.D. degree from Gazi University. He is currently working as Professor at the Kütahya Dumlupınar University. His research focuses on solid-state physics, Bain transformations, magnetic materials.

Yasin Göktürk Yıldız received his M.S. and Ph.D. degrees in Physics from the Kırıkkale University. He is currently working as Associate Professor at the Kırıkkale University. His research focuses on characterization of phase transformations, magnetism, nanoscale modeling, effective field theory.

Gökçen Dikici Yıldız received M.S. and Ph.D. degrees in Physics from the Kırıkkale University. She is currently working as Associate Professor at the Kırıkkale University. Her research focuses on phase transformations, alloys, density functional theory, effective field theory.

Nermin Kahveci Yağcı received M.S. and Ph.D. degrees in Physics from the Ondokuz Mayıs University. She is currently working as Associate Professor at the Kırıkkale University. Her research focuses on crystal structure, magnetic materials, density functional theory, effective field theory.